Reduced Cost of Reactive Power in Doubly Fed Induction Generator Wind Turbine System With Optimized Grid Filter

Dao Zhou, *Member, IEEE*, Frede Blaabjerg, *Fellow, IEEE*, Toke Franke, *Member, IEEE*, Michael Tonnes, and Mogens Lau

***Abstract*—The modern grid requirement has caused that the wind power system behaves more like conventional rotating generators, and it is able to support certain amount of the reactive power. For a typical doubly fed induction generator (DFIG) wind turbine system, the reactive power can be supported either through the rotor-side converter or the grid-side converter. This paper first compares the current ripples and supportive reactive power ranges between the conventional *L* and optimized *LCL* filter, if the reactive power is injected from the grid-side converter. Then, the loss distribution is evaluated both for the generator and the wind power converter in terms of the reactive power done by the rotor-side converter or the grid-side converter with various grid filters. Afterward, the annual energy loss is also estimated based on yearly wind profile. Finally, experimental results of the loss distribution are performed in a down-scaled DFIG system. It is concluded that overexcited reactive power injected from the grid-side converter has lower energy loss per year compared to the overexcited reactive power covered by the rotor-side converter. Furthermore, it is also found that the annual energy loss could even become lower with the optimized filter and thereby more energy production for the wind turbine.**

***Index Terms*—Cost-of-energy, DFIG, loss dissipation, reactive power.**

I. Introduction

THE voltage-source converter is widely used as an interface for the renewable energy systems before they are linked to the grid like in the photovoltaic and wind power system cases, with its advantages in fully control of dc-link voltage, active and reactive power, as well as power factor [1]–[3]. A grid filter is normally introduced to avoid the pulse width modulation carrier and side-band voltage harmonics coupling to the grid that can disturb other sensitive loads or equipment. For the megawatt-level wind power converter, due to the quite low switching frequency of the power switching devices (usually several kilohertz), a simple filter inductor consequently becomes bulky, expensive, and it may also bring poorer dynamics into the system [4]–[6].

In order to fulfill the modern grid codes [7]–[9], the wind turbine system is currently required to behave more like a traditional power source (e.g., synchronous generator), which implies that the wind turbine system should have the capability of reactive power support. Due to the doubly fed mechanism of the doubly fed induction generator (DFIG)-based wind turbine system, the reactive power can be supported either by the grid-side converter (GSC) or the rotor-side converter (RSC). If the reactive power is provided by the GSC, in the case of the constant dc-link voltage, the modulation index is closely related to the filter inductance, and it will increase very fast to overmodulation, especially when overexcited (OE) reactive power is needed [10]. There are two ways to deal with this issue—increase the dc-link voltage, which gives higher switching loss and power rating, or design an optimized grid filter.

Besides, if a small amount of reactive power is demanded by the transmission system operator, it is also of interest to compare the loss of the whole DFIG system, as the reactive power supported by the GSC only affects the loss of the GSC, while the reactive provided by the RSC not only influences the loss of the RSC, but also the loss of the generator itself. Then, the annual energy loss of the wind turbine system and cost of the reactive power can be calculated based on the annual wind profile at different compensation schemes.

The structure of this paper is organized as follows. Section II addresses the function of the grid filter in terms of the grid current ripple and the reactive power range. Then, the *LCL* filter design procedure and the characteristic comparison between the *L* filter and the *LCL* filter are discussed in Section III. The loss model and loss distribution of the DFIG system in the case of OE reactive power injection is followed in Section IV. According to an annual wind profile, Section V discusses the energy loss per year. Finally, after the loss distribution of different parts in the DFIG system is measured on a 7.5-kW test rig in Section VI, some concluding remarks are drawn in Section VII.

II. Functions of Grid Filter

One of the most popular concepts in the mainstream wind power system market is the DFIG configuration as shown in Fig. 1. Except for the advantage that the back-to-back power converters take up only the slip power of the DFIG, this configuration has two possibilities to deliver the demanded reactive

Manuscript received October 2, 2014; accepted November 16, 2014. Date of publication November 26, 2014; date of current version May 22, 2015. Recommended for publication by Associate Editor M. Molinas.

D. Zhou and F. Blaabjerg are with the Department of Energy Technology, Aalborg University, DK-9220 Aalborg, Denmark (e-mail: zda@et.aau.dk; fbl@et.aau.dk).

T. Franke and M. Tonnes are with Danfoss Silicon Power GmbH, 24941 Flensburg, Germany (e-mail: toke.franke@danfoss.com; michael.tonnes@danfoss.com).

M. Lau is with Siemens Wind Power A/S, 7330 Brande, Denmark (e-mail: mogens.lau@siemens.com).

Color versions of one or more of the figures in this paper are available online at http://ieeexplore.ieee.org.

Digital Object Identifier 10.1109/TPEL.2014.2374652

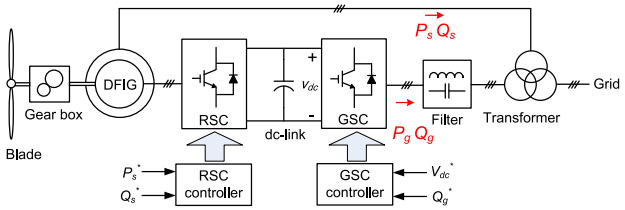

Fig. 1. Typical DFIG configuration in a wind turbine system (GSC: grid-side converter; RSC: rotor-side converter).

TABLE I
BASIC PARAMETERS OF A 2-MW DFIG SYSTEM

Rated power P_s	2 MW
Range of DFIG rotor speed n_r	1050–1800 r/min
Line frequency f_1	50 Hz
Rated line voltage amplitude U_{gm}	563 V
DC-link voltage U_{dc}	1050 V
Switching frequency f_s	2 kHz

power, either from the generator's stator Q_s controlled by the RSC or from the GSC Q_g [10]. Since the inductance difference for the secondary and tertiary winding of the three-winding transformer affects the amount of reactive power transmitted to the power grid, the three winding ratio is assumed as 1:1:1 for simplicity. The control of the back-to-back power converter is described in [11].

As recommended in IEEE 519-1992, harmonics higher than 35th should be explicitly limited [12]. If a simple L filter is assumed to be used, the current ripple amplitude is jointly decided by the dc-link voltage, the switching frequency, and inductance value [13]. For a typical 2-MW DFIG-based wind turbine system, the main parameters of which are listed in Table I, the relationship between the current ripple and the active power of GSC P_g is shown in Fig. 2(a). It is noted that as expected the higher inductance is, the lower switching current ripple will be.

As aforementioned, if the reactive power is required from the grid, the value of the filter inductance also affects the modulation index. Fig. 2(b) indicates the relationship between the dc-link voltage and the reactive power of the GSC Q_g (the fully modulation index is assumed). In order to fulfill the reactive power range stated in E.ON Netz [7], the DFIG system should cover up to 0.4 p.u. OE and 0.3 p.u. underexcited (UE) reactive power in respect to the generator power rating. As the p.u. value is normally defined by the power rating of the induction generator, the used p.u. value in Fig. 2(b) becomes 2.0 p.u. OE and 1.5 p.u. UE reactive power in respect to the GSC, which is five times higher than the p.u. value seen from the induction generator due to the rated slip power through the GSC. It can be seen that the minimum dc-link voltage increases considerably with higher inductance if the OE reactive power is needed. On the other hand, the higher inductance results in a lower switching ripple. Thus, it is a tradeoff procedure of the grid filter design. For the DFIG system as shown in Fig. 1, since the final current ripple to the power grid is calculated as the sum of the stator current and the GSC current, and the stator current is much higher than the GSC current, 40% current ripple at the GSC is acceptable

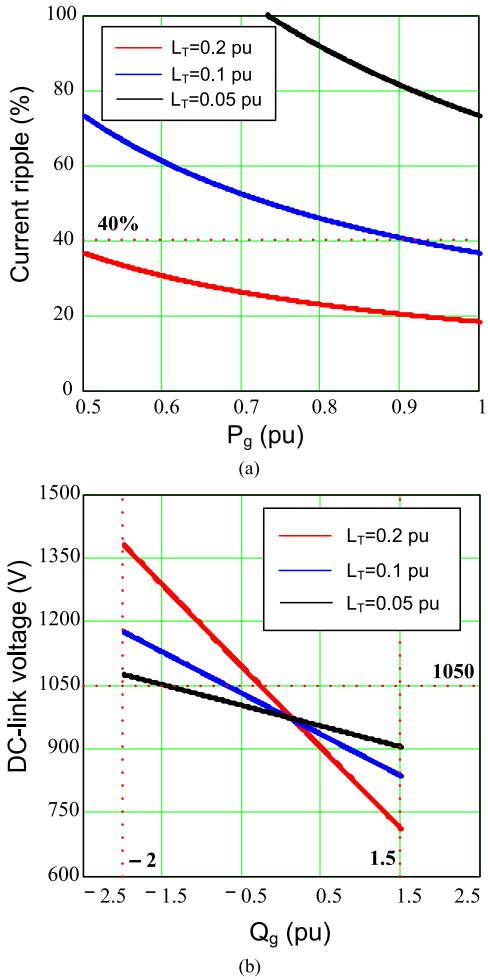

Fig. 2. Influence of grid filter inductance on the GSC performance. (a) Current ripple rate. (b) Reactive power range.

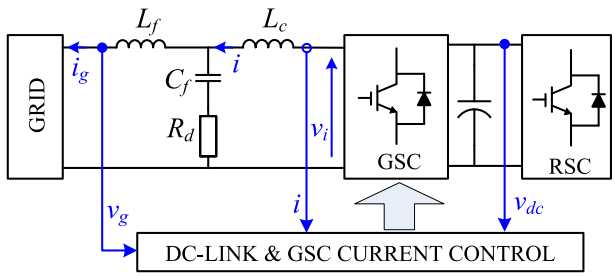

Fig. 3. Equivalent single-phase GSC with *LCL* filter.

and it is used as the design criteria, which implies that the filter inductance is selected at 0.1 p.u.

III. CHARACTERISTIC COMPARISON OF AN *L* AND *LCL* FILTER

The equivalent single-phase GSC with an *LCL* filter is shown in Fig. 3, which typically has no additional sensors compared to the conventional *L* filter configuration. Although the different positions of the voltage and current sensors may have their own advantages [13], the current sensors on the converter side

TABLE II
L AND *LCL* FILTER PARAMETERS

L filter	Filter inductor L_l	500 μH
LCL filter	Converter-side inductor L_c	125 μH
	Grid-side inductor L_f	125 μH
	Filter capacitor C_f	220 μF
	Damping R_d	0.5 mΩ

are chosen, because it can be designed to protect the power semiconductor and it is commonly used in industrial application.

A. Design Procedure of an LCL Filter

As shown in Fig. 3, L_c is the converter-side inductance, L_f is the grid-side inductance, and C_f is the capacitor bank, which is connected to a damping resistance R_d. The converter current and the grid current are represented by i and i_g. Moreover, the voltage of the converter output and the point of common coupling are represented by v_i and v_g, respectively.

A step-by-step design procedure for the *LCL* filter is described in [3]. This design is focused on that the total inductance of the *LCL* filter is able to reduce to half compared to the *L* filter. Afterward, a proper inductance sharing into L_c (0.025 p.u.) and L_g (0.025 p.u.) is realized in order to achieve the desired current ripple reduction. The capacitance value (0.1 p.u.) is then determined by the absorbed reactive power at the rated conditions, in which the resonant frequency becomes 1.35 kHz (67.5% of $f_{\rm sw}$). The passive damping is inevitably designed to overcome the resonant problem, where its power dissipation is also taken into account [3], [13]–[15]. The used filter parameters are summarized in Table II.

B. Characteristic Comparison Between L and LCL Filters

If the transfer function of the PI current controller, the modulation unit, as well as some delays introduced by the digital control are considered, the open-loop Bode plots of the *L* and the *LCL* filter from the GSC current reference to the line current are then shown in Fig. 4. It is clear that the magnitude and phase characteristic between the *L* and *LCL* filters are exactly the same at lower frequency, if the PI parameter used in the current controller is under proper design. It is also noted that the smaller magnitude of the *LCL* filter appears at the switching frequency compared to the *L* filter. Moreover, the damping of the *LCL* filter has a better performance compared to the *L* filter above the switching frequency as expected.

IV. LOSS BREAKDOWN OF THE DFIG SYSTEM

The reactive power injection basically consists of the OE reactive power and the UE reactive power. As analyzed in [16], the specific OE reactive power injection decreases the efficiency of the DFIG system. Consequently, only this kind of reactive power operation is in focus in this paper.

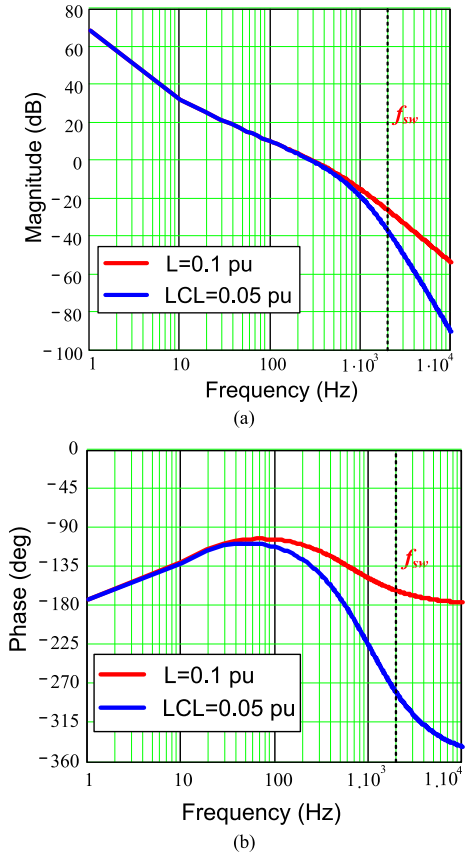

Fig. 4. Bode plot comparison between pure *L* filter (0.1 p.u.) and designed *LCL* filter (0.05 p.u.). (a) Magnitude diagram. (b) Phase diagram.

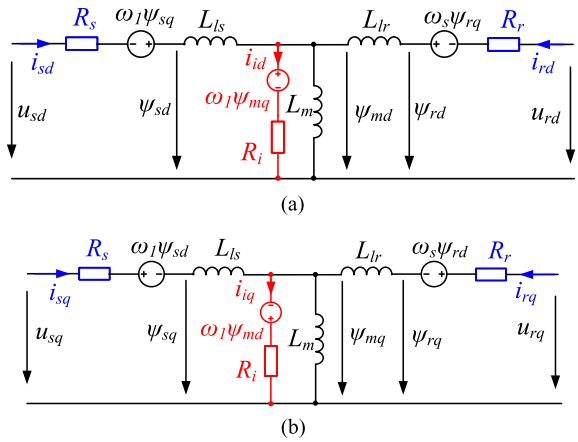

Fig. 5. DFIG equivalent circuit considering copper loss and iron loss. (a) *d*-axis circuit. (b) *q*-axis circuit.

A. Loss Model of the DFIG System

As shown in Fig. 1, the common-adopted methodology to compensate the reactive power is from the stator of the induction generator, due to the fact that it introduces a small increase of the rotor-side current because of the winding ratio between the stator and the rotor of the DFIG [17]. However, this approach not only affects the loss of the RSC, but also imposes the loss of the DFIG itself.

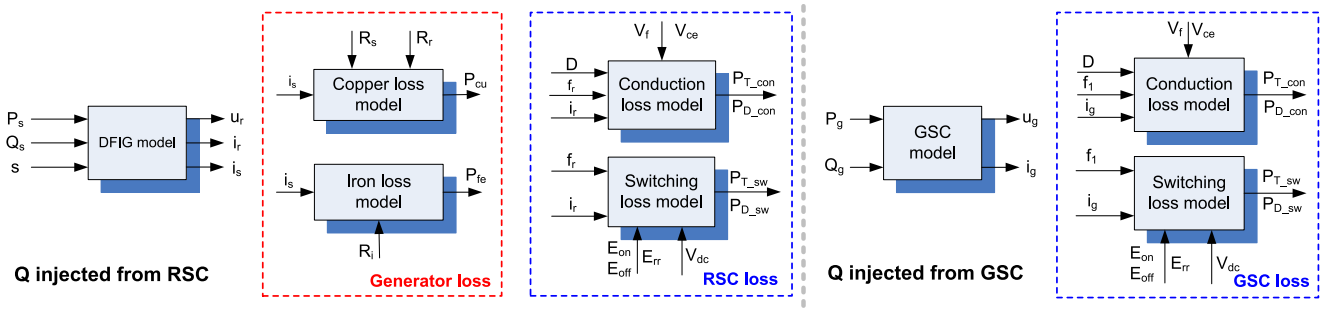

Fig. 6. Framework of power loss estimation. (a) Reactive power is injected by the RSC. (b) Reactive power is injected by the GSC.

TABLE III
CASES FOR NOR AND OVEREXCITED REACTIVE POWER INJECTION

	Q_s (p.u.)	Q_g (p.u.)	U_{dc} (V)
NOR	0	0	1050
OE_RSC	0.4	0	1050
OE_L_GSC	0	0.4	1250
OE_LCL_GSC	0	0.4	1100

Loss dissipation inside the induction generator generally consists of the copper loss and iron loss as shown in Fig. 5 [18]. If the stator voltage-oriented vector control is applied, the stator-side active power P_s and reactive power Q_s are independently in line with the stator d-axis current i_{sd} and q-axis current i_{sq}. Due to the flux equation existing in the DFIG, the relationship between the rotor and stator current under d-axis and q-axis is

$$\begin{cases} i'_{rd} = -\dfrac{L_{ls}+L_m}{L_m} i_{sd} \\ i'_{rq} = -\dfrac{U_{gm}}{\omega_1 \cdot L_m} - \dfrac{L_{ls}+L_m}{L_m} i_{sq} \end{cases} \tag{1}$$

where L_{ls} and L_m denote the stator leakage inductance and the magnetizing inductance, U_{gm} denotes the rated grid phase voltage, ω_1 is the fundamental electrical angular frequency, and the subscript d and q denote the value at d-axis and q-axis circuit, respectively.

The copper loss $P_{\rm cu}$ is resistive losses occurring in the winding coils and can be calculated using the equivalent dq axis circuit stator resistance R_s and rotor resistance R_r as shown in Fig. 5

$$P_{\rm cu} = \frac{3}{2} \cdot [(i_{sd}^2 + i_{sq}^2) \cdot R_s + (i_{rd}^2 + i_{rq}^2) \cdot R_r] \tag{2}$$

where i_s and i_r denote the stator current and the rotor current, respectively. It can be seen that the copper loss of the induction generator is jointly dependent on the stator active power and reactive power.

Generally, the iron loss is produced by the flux change, and it consists of eddy current loss and hysteresis loss, both of which are tightly connected with the operation frequency and flux density [18]. This method needs to know the empirical formula in advance, and the calculation is normally done according to the finite-element method. Alternatively, iron losses can be estimated from the electrical point of view [19], [20]. In other words, it can be expressed by the equivalent iron resistance R_i in parallel with the magnetizing inductance as shown in Fig. 5.

The voltage equations for the additional iron resistor are

$$\begin{cases} R_i \cdot i_{id} = \dfrac{d\psi_{md}}{dt} - \omega_1 \cdot \psi_{mq} \\ R_i \cdot i_{iq} = \dfrac{d\psi_{mq}}{dt} + \omega_1 \cdot \psi_{md} \end{cases} \tag{3}$$

where i_i is the equivalent iron loss current and ψ_m is the magnetizing flux. Moreover, with the aid of the relationship between the stator flux and magnetizing flux

$$\begin{cases} \psi_{md} = \psi_{sd} - L_{ls} \cdot i_{sd} \\ \psi_{mq} = \psi_{sq} - L_{ls} \cdot i_{sq} \end{cases} \tag{4}$$

where ψ_s denotes the stator flux.

Due to the stator voltage orientation, ψ_{md} is nearly zero, and ψ_{mq} is a constant value because of the stiff grid with the constant voltage and constant frequency. Substituting (4) into (3), the iron current can be deduced

$$\begin{cases} i_{id} = \dfrac{\omega_1 L_{ls}}{R_i} \cdot i_{sq} + \dfrac{U_{gm}}{R_i} \\ i_{iq} = -\dfrac{\omega_1 L_{ls}}{R_i} \cdot i_{sd}. \end{cases} \tag{5}$$

According to (5), it is noted that the d-axis iron loss current depends on the reactive power Q_s, while the q-axis iron loss current is related to the active power P_s. As a consequence, the iron loss $P_{\rm fe}$ can be calculated as

$$P_{\rm fe} = \frac{3}{2} \cdot [(i_{id}^2 + i_{iq}^2) \cdot R_i]. \tag{6}$$

In respect to the losses of the power converters in the DFIG system, it is well described in [16]. If the reactive power is provided by the RSC, the loss model of the generator (copper loss and iron loss) and the RSC (conduction loss and switching loss both in the IGBT and the freewheeling diode) is shown in Fig. 6(a). It is evident that if the references of the active power, reactive power, and slip are known in advance, together with the information of the generator and power switching devices, each type of the losses can be analytically calculated.

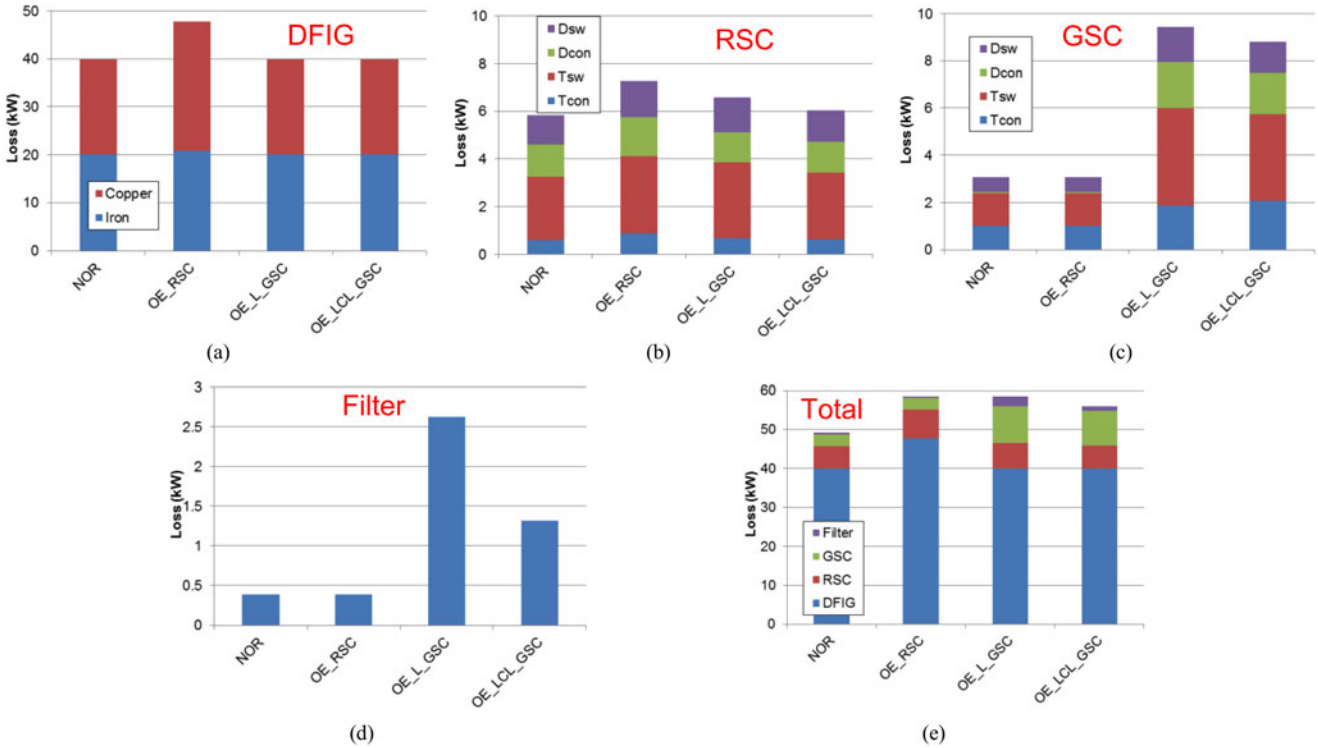

Fig. 7. Loss breakdown at rated wind speed (11 m/s) with various reactive power compensation schemes. (a) DFIG itself. (b) RSC. (c) GSC. (d) Grid filter. (e) Total system.

With the aid from the GSC, another approach may be realized to compensate the reactive power, which stresses the GSC and affects the loss of the GSC and the filter. Compared with the GSC losses, the grid filter loss is small enough [21], and it is simply calculated by its parasitic equivalent series resistance (ESR). Similarly, as the conduction loss and switching loss of the IGBT and the diode are analytically solved, the GSC loss can be calculated as shown in Fig. 6(b).

B. Loss Breakdown of the DFIG System

The loss distribution of the whole DFIG system is first evaluated at the normal operation (NOR), i.e., no reactive power is exchanged between the DFIG system and the grid. Then, the loss distribution is given in cases that the OE reactive power is fully from the RSC (OE_RSC) or the GSC. As the type of the grid filter only influences the loading of the GSC, it can be further divided by *L* filter (OE_L_GSC) and *LCL* filter (OE_LCL_GSC). The above cases are summarized in Table III. It is worth to mention that the dc-link voltage can be different at various compensation schemes which is consistent with Fig. 2(b). It can be seen that the OE_L_GSC has a higher dc voltage than the OE_LCL_GSC, due to the higher total inductance of the filter.

The loss breakdown at the rated power of the four cases in terms of the DFIG, the RSC, the GSC, and its filter is then shown in Fig. 7. In respect to the generator loss, together with the parameters of the DFIG listed in Table IV, it can be seen that the generator losses (especially copper losses) increase only in the OE_RSC compared to the NOR in Fig. 7(a), because the reactive power injection by the RSC changes the generator's stator and rotor current amplitude. In respect to the RSC losses, it also increases considerably in the OE_RSC. Moreover, the power loss (especially the switching loss) increases slightly in OE_L_GSC and OE_LCL_GSC compared to the NOR operation, since the dc-link voltage becomes higher. For the GSC losses, OE_RSC stays the same with the NOR operation. However, if the reactive power is supported by the GSC, both the conduction losses and the switching losses increase significantly because of the dominating reactive current, and it also becomes three times higher than in the case that the reactive power is injected by the RSC. The tendency of the grid filter loss is similar to the GSC because of the same current through them. It is noted that if the OE reactive power is compensated from the GSC, the *LCL* filter consumes lower power loss due to the smaller ESR compared to the pure *L* filter. For the loss distribution of the whole DFIG

TABLE IV
2-MW GENERATOR AND BACK-TO-BACK POWER CONVERTER

Generator	Rated power P_s	2 MW
	Rated line voltage U_{sm}	563 V
	Stator leakage inductance L_{ls}	0.050 p.u.
	Rotor leakage inductance L_{lr}	0.085 p.u.
	Magnetizing inductance L_m	3.840 p.u.
	Stator resistance R_s	0.007 p.u.
	Rotor resistance R_r	0.006 p.u.
	Equivalent iron loss resistance R_i	99.853 p.u.
	Ration of stator and rotor winding	0.369
Power converters	Used power module	1 kA/1.7 kV
	Grid-side converter	Single
	Rotor-side converter	Two in parallel

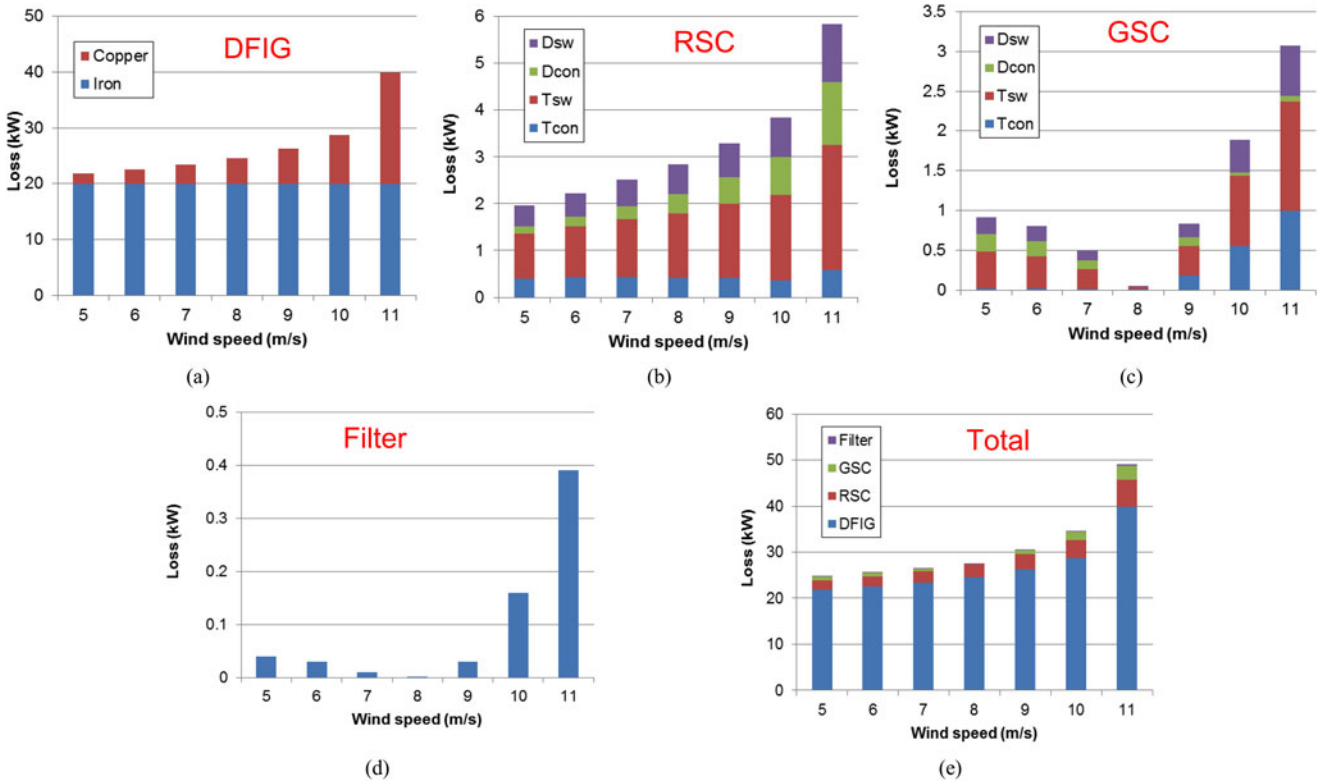

Fig. 8. Loss breakdown at NOR with different wind speeds. (a) DFIG itself. (b) RSC. (c) GSC. (d) Grid filter. (e) Total system.

system, compared with the loss of the DFIG itself and the power converters, the loss dissipated in the DFIG is dominant.

From another perspective, if no reactive power is required, the power loss of various parts in the DFIG system at different wind speeds is shown in Fig. 8 (assuming that after 11-m/s wind turbine is operating at full load). In Fig. 8(a), it is noted that the iron loss stays almost constant at various wind speeds, while the copper loss changes dynamically. For the RSC losses shown in Fig. 8(b), it increases with the higher wind speed. With respect to the GSC losses at different wind speeds, it can be seen that the power loss becomes low at 8 m/s, which is regarded as the synchronous operation as shown in Fig. 8(c). The loss of the grid filter is much smaller than the GSC as shown in Fig. 8(d). Besides, the loss distribution of the whole DFIG system is shown in Fig. 8(e).

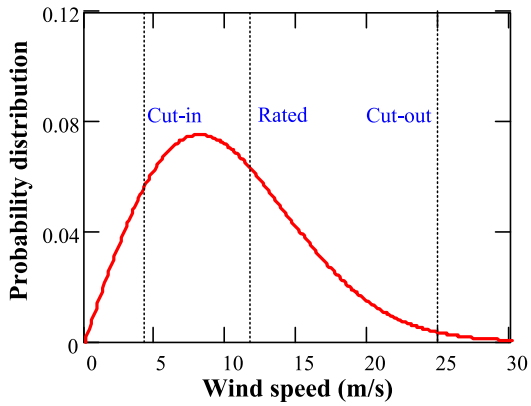

Fig. 9. Class I annual wind distribution defined by IEC standard [22].

V. Energy Loss Based on Annual Wind Profile

Based on the power loss model and the loss distribution with various amounts of reactive power described in Section IV, this section further estimates the energy loss and cost of reactive power according to an annual wind profile.

The annual wind of Weibull distribution according to the IEC standard-Class I [22], [23] with the mean wind speed 10 m/s is shown in Fig. 9. As each loss (kW) at various wind speeds can be calculated by a wind speed step of 1 m/s as shown in Fig. 8, as well as the yearly wind speed distribution (hours), the annual loss of energy can be calculated. It is worth to mention that the annual loss of energy is only concerned from the cut-in to the rated wind speed, because if the wind speed is higher than rated value, it is assumed that the power loss dissipated (loss of energy production) in the DFIG system can be compensated by the mechanical power from the wind turbine blades.

The annual energy loss of the DFIG system at various operation modes is shown in Fig. 10(a). It is evident that the energy consumed by the induction generator is much higher than in the back-to-back power converters. Moreover, it can be seen that although the OE reactive power compensation from the GSC significantly imposes the loading of the GSC itself and its filter, the OE_LCL_GSC still has the lowest loss of energy.

It is also an interesting perspective to express the annual energy loss in terms of the percentage over the yearly produced

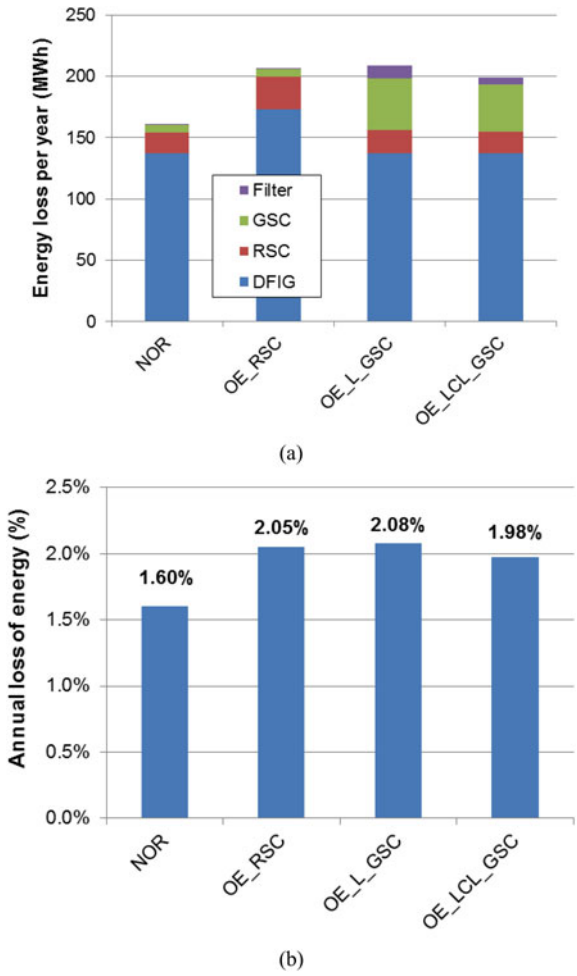

Fig. 10. Annual loss of energy in NOR and if the OE reactive power is required all year around. (a) Energy loss per year (MWh). (b) Annual loss of energy (%).

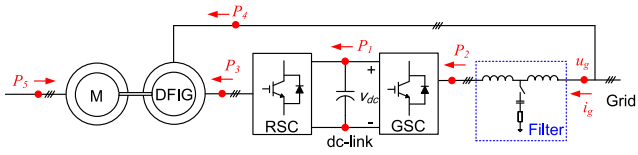

Fig. 11. Setup of 7.5-kW DFIG test rig.

energy, which is accumulated from the cut-in until the cutoff wind speed. As shown in Fig. 10(b), under the assumption that the OE reactive power is required all year around, the normal case is the OE_RSC that takes up 2.05% annual energy, while the best situation is achieved by the OE_LCL_GSC 1.98%, which implies 3.41% energy saving per year.

VI. Experimental Verification of Loss Dissipation

In order to validate the loss dissipation of the DFIG system at different reactive power compensation methods, a down-scaled 7.5 kW test rig is built up and shown in Fig. 11. The DFIG is externally driven by a prime motor, and two 5.5-kW Danfoss motor drives are used for the GSC and the RSC, both of which

TABLE V
7.5-kW Generator and 5.5-kW Back-to-Back Power Converter

Generator	Rated power	7.5 kW
	Rated line voltage	380 V
	Stator leakage inductance	0.056 p.u.
	Rotor leakage inductance	0.084 p.u.
	Magnetizing inductance	1.294 p.u.
	Stator resistance	0.022 p.u.
	Rotor resistance	0.033 p.u.
	Equivalent iron loss resistance	35.734 p.u.
	Ratio of stator and rotor winding	0.336
Power converters	Rated power	5.5 kW
	Grid-side converter rated current	10 A
	Rotor-side converter rated current	10 A
	Switching frequency	5 kHz
Grid filters	L type	
	Interface inductance L_l	5.9% p.u.
	LCL type	
	Converter-side inductor L_c	3.6% p.u.
	Grid-side inductor L_f	2.3% p.u.
	Filter capacitor C_f	20.0% p.u.
	Damping R_d	13.4% p.u.

are controlled with dSPACE 1006. Besides, the *LCL* filter is employed as the grid filter, whose capacitor branch can be bypassed to realize the *L*-type filter. The important parameters of the test setup are summarized in Table V. It is noted that, as the rated rotor speed is 1800 r/min, the p.u. value of the grid filter is calculated based on the slip power of the DFIG.

In the condition that the full power of the DFIG is realized at 1800 r/min, 0.4-p.u. reactive power according to the grid codes is compensated from the GSC; the current injecting to the grid from the back-to-back power converter is compared with the *LCL* and *L* filter as shown in Fig. 12. It is noted that the fundamental currents of the *L* and the *LCL* filter both are 4.2 A, and the currents are leading the grid voltage 90°, as the majority of which belongs to the reactive component. Furthermore, the maximum value of the harmonic spectrum around the switching frequency is 105 mA with the *L* filter, which is much higher than the *LCL* filter 25 mA.

The loss dissipation of the various parts in the down-scaled DFIG system is monitored by Yokogawa Power Analyzer WT3000. The loss of the DFIG itself, the RSC, the GSC and the grid filter are tested separately and they are shown in Fig. 13, in which four conditions are taken into account consistent with Fig. 7. It is worth to mention that the dc-link used in the above four cases is 600, 600, 750, and 650 V, respectively. In respect to the loss of the DFIG itself and the RSC, it consumes the highest in the case that the reactive power is compensated from the RSC. However, regarding the GSC, the reactive power supported by the GSC with the *L* filter leads to the highest power loss, and similar filter loss can be observed in the cases of the reactive power compensation by the GSC because of the same value between the *L* and *LCL* filters.

The experimental result of total loss dissipation in the DFIG system at 1800 r/min is then shown in Fig. 14. Compared with Fig. 7(e), since the loss consumed in the DFIG actually contains both the DFIG loss and prime motor loss, the loss distribution of the DFIG is much higher compared to power converters. Moreover, it can be seen that the both OE_L_GSC and OE_LCL_GSC

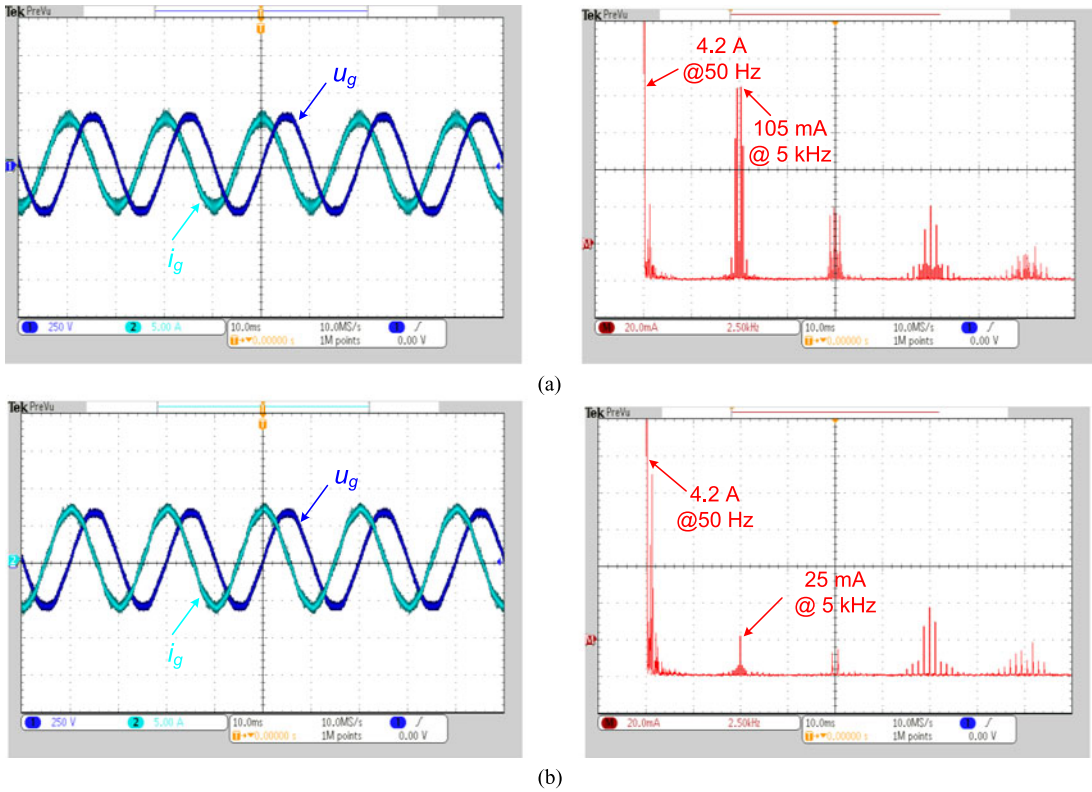

Fig. 12. Waveform and the harmonic of the grid current. (a) *L* filter. (b) *LCL* filter.

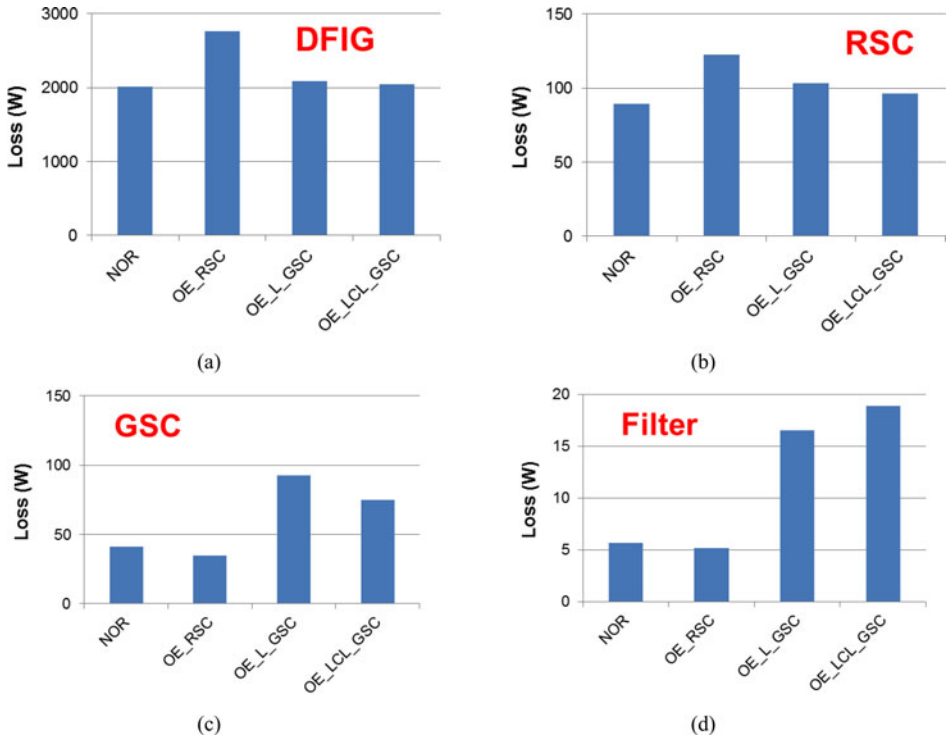

Fig. 13. Measured loss dissipation in the DFIG system at 1800 r/min in the case of the NOR and the various reactive power compensation schemes. (a) DFIG itself. (b) RSC. (c) GSC. (d) Grid filter.

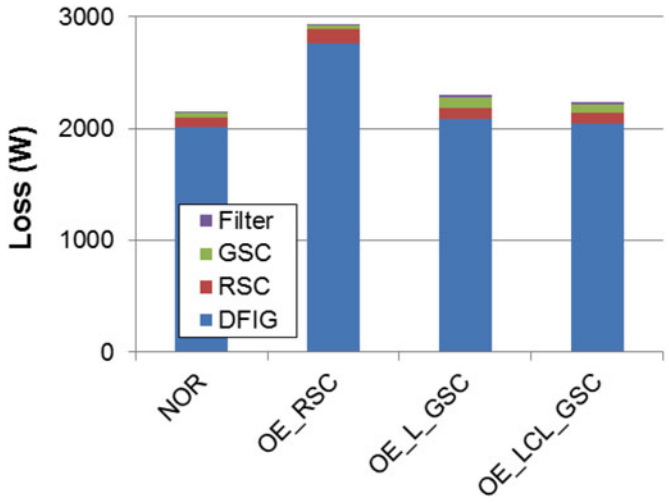

Fig. 14. Experimental result of total loss dissipation in the DFIG system at 1800 r/min in the case of the NOR and the various reactive power compensation schemes.

are more efficient than OE_RSC due to the different amounts of the equivalent loss resistors between the 2-MW and 7.5-kW DFIGs.

VII. Conclusion

This paper has studied the influence of the grid filter inductance on the current ripple and the reactive power range for a DFIG wind turbine system. Then, an optimized *LCL* filter design is achieved with half value of the total inductance compared to the pure *L* filter.

Due to the existence of the two possibilities to generate the demanded reactive power for the DFIG system—controlled by the RSC or controlled by the GSC—each of them is analyzed in terms of the DFIG loss and the power converters loss. It is concluded that although the compensation from the GSC significantly increases the power loss of the GSC itself, it will still have lower total loss dissipation of the whole DFIG system, as the compensation approach by the RSC will impose the DFIG loss as well as the RSC loss.

Based on a typical annual wind speed distribution, the loss of energy per year is finally discussed. It can be seen that the injection of reactive power is actually not free of charge. Assuming that the cost the offshore wind power is 0.2 Euro/kWh, compared with the NOR of 1.60% annual energy loss (32.2k Euro), if the OE reactive power is injected by the RSC, it will increase to 2.05% annual energy loss (41.3k Euro) when the reactive power is needed all year around. On the other hand, if the grid filter is properly designed and the OE reactive power is supported by the GSC, the annual energy loss becomes 1.98% (39.7k Euro), which implies 3.41% (1.6k Euro) energy saving per year compared to the OE reactive injected by the RSC.

References

[1] A. A. Rockhill, M. Liserre, R. Teodorescu, and P. Rodriguez, "Grid-filter design for a multi-megawatt medium-voltage voltage-source inverter," *IEEE Trans. Ind. Electron.*, vol. 58, no. 4, pp. 1205–1217, Apr. 2011.

[2] M. Liserre, F. Blaabjerg, and A. Dell'Aquila, "Step-by-step design procedure for a grid-connected three-phase PWM voltage source converter," *Int. J. Electron.*, vol. 91, no. 8, pp. 445–460, Jan. 2004.

[3] M. Liserre, F. Blaabjerg, and S. Hansen, "Design and control of an LCL-filter-based three-phase active rectifier," *IEEE Trans. Ind. Appl.*, vol. 41, no. 5, pp. 1281–1291, Sep. 2005.

[4] Z. Chen, J. M. Guerrero, and F. Blaabjerg, "A review of the state of the art of power electronics for wind turbines," *IEEE Trans. Power Electron.*, vol. 24, no. 8, pp. 1859–1875, Aug. 2009.

[5] F. Blaabjerg, Z. Chen, and S. B. Kjaer, "Power electronics as efficient interface in dispersed power generation systems," *IEEE Trans. Power Electron.*, vol. 19, no. 5, pp. 1184–1194, Sep. 2004.

[6] M. Liserre, R. Cardenas, M. Molinas, and J. Rodriguez, "Overview of multi-MW wind turbines and wind parks," *IEEE Trans. Ind. Electron.*, vol. 58, no. 4, pp. 1081–1095, Apr. 2011.

[7] *Requirements for Offshore Grid Connections*, E. ON-Netz, Dusseldorf, Germany, Apr. 2008.

[8] M. Tsili and S. Papathanassiou, "A review of grid code technical requirements for wind farms," *IET Renewable Power Gener.*, vol. 3, no. 3, pp. 308–332, Sep. 2009.

[9] A. Camacho, M. Castilla, J. Miret, R. Guzman, and A. Borrell, "Reactive power control for distributed generation power plants to comply with voltage limits during grid faults," *IEEE Trans. Power Electron.*, vol. 29, no. 11, pp. 6224–6234, Nov. 2014.

[10] D. Zhou, F. Blaabjerg, M. Lau, and M. Tonnes, "Thermal behavior optimization in multi-MW wind power converter by reactive power circulation," *IEEE Trans. Ind. Appl.*, vol. 50, no. 1, pp. 433–440, Jan. 2014.

[11] S. Muller, M. Deicke, and R. W. De Doncker, "Doubly fed induction generator systems for wind turbines," *IEEE Ind. Appl. Mag.*, vol. 8, no. 3, pp. 26–33, May 2002.

[12] A. Nagel and R. W. De Doncker, "Systematic design of EMI-filters for power converters," in *Proc. Conf. Rec. Ind. Appl. Conf.*, 2000, pp. 2523–2525.

[13] R. Teodorescu, M. Liserre, and P. Rodriguez, *Grid Converters for Photovoltaic and Wind Power Systems*. Hoboken, NJ, USA: Wiley, 2011.

[14] R. Pena-Alzola, M. Liserre, F. Blaabjerg, R. Sebastian, J. Dannehl, and F. W. Fuchs, "Analysis of the passive damping losses in LCL-filter-based grid converters," *IEEE Trans. Power Electron.*, vol. 28, no. 6, pp. 2642–2646, Jun. 2013.

[15] W. Wu, Y. He, T. Tang, and F. Blaabjerg, "A new design method for the passive damped LCL and LLCL Filter-based single-phase grid-tied inverter," *IEEE Trans. Ind. Electron.*, vol. 60, no. 10, pp. 4339–4350, Oct. 2013.

[16] D. Zhou, F. Blaabjerg, M. Lau, and M. Tonnes, "Thermal cycling overview of multi-megawatt two-level wind power converter at full grid code operation," *IEEJ J. Ind. Appl.*, vol. 2, no. 4, pp. 173–182, Jul. 2013.

[17] S. Engelhardt, I. Erlich, C. Feltes, J. Kretschmann, and F. Shewarega, "Reactive power capability of wind turbines based on doubly fed induction generators," *IEEE Trans. Energy Convers.*, vol. 26, no. 1, pp. 364–372, Mar. 2011.

[18] R. Takahashi, H. Ichita, J. Tamura, M. Kimura, M. Ichinose, M. Futami, and K. Ide, "Efficiency calculation of wind turbine generation system with doubly-fed induction generator," in *Proc. Int. Conf. Electr. Mach.*, 2010, pp. 1–4.

[19] S. Wee, M. Shin, and D. Hyun, "Stator-flux-oriented control of induction motor considering iron loss," *IEEE Trans. Ind. Electron.*, vol. 48, no. 3, pp. 602–608, Jun. 2001.

[20] A. G. Abo-Khalil, H. Park, and D. Lee, "Loss minimization control for doubly-fed induction generators in variable speed wind turbines," in *Proc. 33rd Annu. Conf. Ind. Electron. Soc.*, 2007, pp. 1109–1114.

[21] C. Sintamarean, F. Blaabjerg, and H. Wang, "Comprehensive evaluation on efficiency and thermal loading of associated Si and SiC based PV inverter applications," in *Proc. Annu. Conf. Ind. Electron. Soc.*, 2013, pp. 555–560.

[22] *Wind Turbines—Part I: Design Requirements*, 3rd ed., 2014, IEC 61400-1.

[23] Vestas website. (2014). [Online]. Available: http://www.vestas.com/en/wind-power-plants/wind-project-planning/siting/wind-classes.aspx?action=3#/vestas-univers)

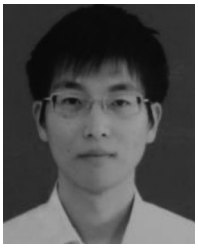

Dao Zhou (S'12–M'14) received the B.Sc. degree in electrical engineering from Beijing Jiaotong University, Beijing, China, in 2007, and the M.Sc. degree in power electronics from Zhejiang University, Hangzhou, China, in 2010. Since 2012, he has been working toward the Ph.D. degree at the Department of Energy Technology, Aalborg University, Aalborg, Denmark.

His research interests include two-level power electronics converters and their application in wind power generation systems.

Frede Blaabjerg (S'86–M'88–SM'97–F'03) received the Ph.D. degree from Aalborg University, Aalborg, Denmark, in 1992.

He was with ABB-Scandia, Randers, Denmark, from 1987 to 1988. He became an Assistant Professor in 1992, an Associate Professor in 1996, and a Full Professor of power electronics and drives in 1998 at Aalborg University. His current research interests include power electronics and its applications such as in wind turbines, PV systems, reliability, harmonics, and adjustable speed drives.

Dr. Blaabjerg has received 15 IEEE Prize Paper Awards, the IEEE Power Electronics Society Distinguished Service Award in 2009, the EPE-PEMC Council Award in 2010, the IEEE William E. Newell Power Electronics Award in 2014, and the Villum Kann Rasmussen Research Award in 2014. He was an Editor-in-Chief of the IEEE TRANSACTIONS ON POWER ELECTRONICS from 2006 to 2012. He was a Distinguished Lecturer for the IEEE Power Electronics Society from 2005 to 2007 and for the IEEE Industry Applications Society from 2010 to 2011.

Toke Franke (M'11) received the Dipl.-Ing. and Ph.D. degrees from Christian-Albrechts-University, Kiel, Germany, in 2007 and 2013, respectively.

Between 2007 and 2011, he carried out research work at Christian-Albrechts-University on silicon carbide power devices in solar applications. From 2011 to 2013, he was a Senior Hardware Technology Engineer at Danfoss Solar Inverters, where he focused on storage technologies and silicon carbide power devices. In 2014, he joined Danfoss Silicon Power GmbH, Flensburg, Germany, as a Senior Engineer for power stacks. His main research interests include power devices and high-density power stacks for renewable energies.

Dr. Franke is a Member of the IEEE Power Electronics Society.

Michael Tonnes received the M.Sc. EE degree from Aalborg University, Aalborg, Denmark, in 1987, and the Ph.D. degree from the Institute of Energy Technology, in 1990.

He was employed by Danfoss in 1987 to perform the Ph.D. work within autotuning and automatic control of nonlinear electrical machines and worked within the technology area of Motor Controls. He worked in the US in Danfoss High Power Drives for the period 1996–1998 and had various management positions within electronic businesses. He is currently a Senior Director of R&D at Danfoss Silicon Power GmbH, Flensburg, Germany. He is an author and co-author of a number of articles on autotuning, motor controls, and power electronics in general and holds several patents in the field of motor controls and power electronics.

Mogens Lau received the M.Sc. degree in electrical engineering from Aalborg University, Aalborg, Denmark, in 1999.

He has worked as a Development Engineer, Project Manager, and Line Manager on power electronics with leading companies like Siemens, Danfoss, Grundfoss, and Vestas. He is currently with Siemens Wind Power A/S, Brande, Denmark.